Determination of the equilibrium enthalpy of melting of two-phase semi-crystalline polymers by fast scanning calorimetry

Clément Fosse, Aurélie Bourdet, Esteve Ernault, Antonella Esposito, Nicolas Delpouve, Laurent Delbreilh, Shanmugam Thiyagarajan, Rutger J.I. Knoop, Eric Dargent

Determination of the equilibrium enthalpy of melting of two-phase semi-crystalline polymers by fast scanning calorimetry

Clément Fosse[a] (clement.fosse1@univ-rouen.fr),

Aurélie Bourdet[a] (aurelie.bourdet@univ-rouen.fr),

Estève Ernault[a] (esteve.ernault@univ-rouen.fr),

Antonella Esposito[a,*] (antonella.esposito@univ-rouen.fr),

Nicolas Delpouve[a] (nicolas.delpouve1@univ-rouen.fr),

Laurent Delbreilh[a] (laurent.delbreilh@univ-rouen.fr),

Shanmugam Thiyagarajan[b] (shanmugam.thiyagarajan@wur.nl),

Rutger J.I. Knoop[b] (rutger.knoop@wur.nl),

Eric Dargent[a] (eric.dargent@univ-rouen.fr)

[a]*Normandie Univ, UNIROUEN Normandie, INSA Rouen, CNRS, Groupe de Physique des Matériaux, 76000 Rouen, France*

[b]*Wageningen Food & Biobased Research, P.O. Box 17, 6700 AA Wageningen, The Netherlands*

[*] Corresponding author antonella.esposito@univ-rouen.fr

ABSTRACT

The equilibrium enthalpy of melting ΔH_m^0 [J·g^{-1}] is an extrapolated thermodynamic quantity attributed to crystallizable macromolecules and widely used to characterize polymers in their semi-crystalline state, for it allows estimating the degree of crystallinity by direct comparison with the enthalpy of melting obtained from differential scanning calorimetry. ΔH_m^0 is typically obtained by cross-comparing the results obtained by at least two techniques. This work proposes a simplified experimental protocol to determine ΔH_m^0 by the use of Fast Scanning Calorimetry (FSC). This approach applies to any crystallizable polymer for which a

specific microstructure can be obtained (i.e. a two-phase semi-crystalline microstructure with a negligible amount of rigid amorphous fraction) and that can also be quenched to its fully amorphous state. Such a two-phase microstructure can be obtained on nanoscale samples through an annealing process performed *in situ* on the FSC sensor at crystallization temperatures as close as possible to the melting temperature. The enthalpy of melting is then evaluated from the two-phase model for different crystallization times (i.e. different crystallinities) and the ΔH_m^0 is obtained by extrapolating the data to the 100% crystalline state. This procedure was applied on samples whose ΔH_m^0 values are already available in the literature, but also on more recent biobased polyesters whose thermal properties are still under investigations.

KEYWORDS

fast scanning calorimetry; rigid amorphous fraction; enthalpy of melting; PEF; PBF

1. INTRODUCTION

Since polymers can crystallize to different extents but never entirely, an extrapolated value of enthalpy, the so-called equilibrium enthalpy of melting ΔH_m^0 [$J \cdot g^{-1}$], can be theoretically defined as the enthalpy that would be obtained from the melting peak of one gram of a 100% crystalline material. According to its own definition, this information is not directly accessible because polymers are made of macromolecules which are way too big to perfectly fold and entirely fit in a regularly repeated crystal lattice; it is however essential to give an estimate of ΔH_m^0, for it allows estimating the degree of crystallinity of a semi-crystalline polymer by direct comparison with the enthalpy of melting measured by DSC for any given semi-crystalline microstructure. The debate is still open on the method used to determine ΔH_m^0, and probably because the method may be different from a research group to another, the values of

ΔH_m^0 found in the literature are sometimes diverging, as shown in Table 1 for a selection of polymers. In addition, some polymers are subjected to polymorphism; to our knowledge, so far only Righetti and co-workers [1] took it into account for the calculation of ΔH_m^0 in the case of poly(lactic acid). Besides, new polymers are continuously synthesized, such as polyfuranoates [2] and many other polyesters, and a value of ΔH_m^0 will certainly have to be found for each of them to make preliminary characterizations complete [3, 4]. It is therefore of great interest to find a method that is robust and efficient to determine the equilibrium enthalpy of melting for semi-crystalline polymers, which would eventually help closing the debate or at least provide further elements for discussion.

Table 1 Values of the equilibrium enthalpy of melting ΔH_m^0 [J·g^{-1}] found in the literature for a selection of crystallizable polymers.

Polymer	**Abbreviation**	ΔH_m^0 **[J·g^{-1}]**
Poly(ethylene)	PE	289 [5], 282 [6], 307 [7], 281 [8]
Isotactic poly(styrene)	iso-PS	86 [9], 80 [10], 96 [11]
Isotactic poly(propylene)	iso-PP	63 [12], 260 [9], 234 [13], 183 [14], 65 [15], 147 [16], 188 [17], 138 [18]
Polyamide 6	PA6	188 [19], 155 [20]
Poly(ethylene terephthalate)	PET	140 [21], 125 [22]
Poly(butylene terephthalate)	PBT	145 [23], 141 [24]
Poly(L-lactic acid)	PLLA	135 [25], 91 [26], 146 [27], 96 [28], 143 (α-crystals) [1], 107 (α'-crystals) [1], $\Delta H_m^0(T) = 20.9 + 0.74T - 0.0011T^2\ [J \cdot g^{-1}]$ for the α'-form and $\Delta H_m^0(T) = 45.7 + 0.74T - 0.0011T^2\ [J \cdot g^{-1}]$ for the α-form [1]
Poly(phenylene sulfide)	PPS	80 [29], 146 [30], 112 [31]
Poly(ethylene 2,5-furandicarboxylate)	PEF	137 [32], 140 [33], 185 [34]
Poly(butylene 2,5-furandicarboxylate)	PBF	129 [35]

Even if some authors estimated the equilibrium enthalpy of melting through methods such as the Flory equation [36] or density measurement [9, 34], the value of ΔH_m^0 for most crystallizable polymers has been more traditionally determined by generating different microstructures with an increasing degree of crystallinity, and then cross-comparing the

results of microstructural characterizations performed by at least two techniques, such as XRD and DSC [1, 27-30, 32-35]. On one side, XRD provides an overall apparent degree of crystallinity that is calculated as a ratio of areas, i.e. the area corresponding to the sharper (crystalline) peaks divided by the total area of the pattern (crystalline peaks plus amorphous halo). On the other side, DSC provides the enthalpy [$J \cdot g^{-1}$] associated to the melting process of the percentage of polymer crystals previously quantified by XRD. A linear regression of several experimental points collected by this method on samples with different crystallinities allows extrapolating the values of enthalpy of melting to the ideal case of a 100% crystalline polymer. Most of the time, the degree of crystallinity X_c is obtained from XRD patterns, the enthalpy of melting ΔH_m is estimated from DSC curves, and the equilibrium enthalpy of melting ΔH_m^0 is calculated according to equation (1).

$$\Delta H_m^0 = \Delta H_m^{DSC} / X_c^{XRD} \quad (1)$$

Sometimes other techniques, such as infrared [8, 36-39] or Raman spectroscopy [40-45], are used to quantify the overall percentage of crystallinity to be compared to the value of enthalpy of melting obtained by DSC, but the use of XRD cross-compared to DSC is by far the most common. In a recent study about PLA, Righetti et al. [1] used XRD patterns cross-compared to conventional DSC to obtain the equilibrium enthalpy of melting as a function of temperature rather than a single extrapolated value. Recently, Cebe et al. [8] proposed a method for determining the equilibrium enthalpy of melting from Fast Scanning Calorimetry (FSC). This method requires the measurement of the enthalpy of melting plotted against the product of the sample mass times its crystallinity for several samples having variable masses and/or crystallinities; in this case, $\Delta H_m{}^0$ is deduced from the slope of the plot, expected to be linear, representing ΔH_m [J] vs. $(m * X_c)$. This method is interesting for it has two major advantages: (1) it allows determining the equilibrium enthalpy of melting for samples that degrade right after melting and therefore can be hardly characterized by conventional DSC

[46-49], and (2) it reduces the uncertainties that could be reproached to conventional DSC, because melting/recrystallization processes are observed at standard heating conditions [48-50] but largely suppressed at higher heating rates [51-55]. According to the authors, this method would reduce errors and can be applied to all types of polymers, copolymers, and blends regardless of their degree of crystallinity. In a paper dealing with the heat capacity of poly(trimethylene terephthalate), Pyda et al. [56] raised the question about the possibility of correlating the heat capacity at the glass transition $\Delta C_p\big|_{T=T_g}$ [J·g^{-1}·mol^{-1}] to the heat of fusion ΔH_f [kJ·mol^{-1}] obtained by calorimetry on the same sample subjected to different thermal treatments (as received, partially quenched, quenched, crystallized isothermally, annealed, after cooling with 10 K·min^{-1}) and therefore with different microstructures and crystallinities. They compared the experimental results to the values predicted on the basis of the ATHAS Data Bank [21] and observed that the extrapolated value of the heat of fusion, which was used as a control over the measured values of heat capacity, was in accord with an extrapolation of the experimental points only when the corresponding microstructure contained little or no rigid amorphous content. The thing is, when it comes to the microstructural description of semi-crystalline polymers, in most cases the two-phase model is better replaced by a more complex three-phase model [57, 58], which involves an additional "phase" to explain the connection between the ordered and disordered domains, the so-called rigid amorphous fraction (RAF). As such, the RAF should be considered as an interphase, rather than a phase, for it usually forms within the amorphous phase and involves all the entangled macromolecular segments that are too disordered to be part of a crystalline domain, yet too constrained by the nearby crystals to relax as freely as the mobile amorphous fraction (MAF). The appearance of a RAF is highly probable, for it is due to the length of the polymer chains, which is intrinsically much larger than the lamellar thickness [59, 60]. The amount of RAF can vary from a polymer to another, sometimes reaching up to 40% [61]. Quite intuitively, the

amount of RAF is expected to decrease if crystals grow bigger and the macromolecular segments get less entangled [58, 60, 62, 63]. Several studies have shown how the RAF can be used to explain some macroscopic properties of semi-crystalline materials [64-70] and understand their behavior [55], which in turns means that controlling the amount of RAF is a key parameter for tailoring the performance of semi-crystalline polymers – almost as much as controlling the global amount, the size and the regularity of the crystalline domains. As pointed out by previous works on the establishment of the RAF [58, 60, 62, 63], the connection between the amorphous and the crystalline domains can be evidenced either during [57, 62, 71, 72] or after the crystallization process [57, 58, 62, 63, 72]. Moreover, the amount of RAF depends on the crystallization conditions (thermal treatment [56, 73], time and temperature of crystallization [55], thickness [74], mechanical treatments [75, 76]). If it is possible to control the amount of RAF by adjusting and carefully controlling the experimental conditions for crystallization, with a suitable set of crystallization parameters it should be possible to eventually create semi-crystalline microstructures in which almost no RAF is formed.

As previously mentioned, the equilibrium enthalpy of melting ΔH_m^0 may be calculated according to equation (1) where X_c is an estimation of the crystallinity degree obtained from XRD patterns, and the enthalpy of melting ΔH_m is calculated from DSC curves. On one side, being part of the amorphous phase, the RAF is expected to contribute to the amorphous halo [77], which should be carefully subtracted to obtain X_c^{XRD}. On the other side, the presence of RAF is known to be responsible for a progressive change in the baseline of the DSC curves [57, 78], which also leads to either overestimate or underestimate ΔH_m^{DSC}, depending on the choice of the baseline and of the temperature range selected for integration. As a consequence, the cross-comparison of X_c^{XRD} with ΔH_m^{DSC} is subjected to large uncertainties on the estimation of ΔH_m^0. Besides, and most importantly, as for any other cross-comparison

126 method, the assumption has to be made that two samples prepared in different ways, having
127 different dimensions, and measured with two different techniques, actually represent the same
128 system. From an experimental point of view, the RAF is distinguished from the MAF as it
129 does not contribute to the heat capacity change at the glass transition [79, 80]. Due to its
130 highly constrained behavior, the "relaxation" of the RAF requires more energy to be
131 accomplished with respect to the relaxation of the MAF, therefore its contribution to the
132 increase in the heat capacity occurs at higher temperatures, contributing to a slight but
133 continuous change in the DSC baseline over the entire temperature range of devitrification
134 [57, 78]. In general, the development of a significant amount of RAF is associated to the
135 growth of irregular crystalline domains [55, 72, 81, 82] that are potentially subjected to
136 crystalline reorganization. As a consequence, most of the time the error made on the
137 estimation of $\Delta H_m^{DSC}$is not only related to the devitrification of the RAF and the choice of a
138 good baseline used to integrate the melting peak, but also to the eventual reorganization
139 (melting/recrystallization) of small and imperfect crystal boundaries [57]. In this case,
140 performing DSC measurements at conventional heating rates (up to 20 K·min^{-1}) exposes to
141 the risk of introducing an additional source of error in the estimation of ΔH_m^{DSC}. FSC is the
142 only experimental technique able to reduce and eventually suppress any contribution due to
143 melting/recrystallization, as shown by Prof. Schick's pioneer work [52-54]. FSC
144 measurements can only be performed if the size of the samples is decreased to nanoscale,
145 within a range of thickness 1-10 μm [83]; Nassar et al. [74] recently observed that
146 crystallizing nanoscale samples in which the polymer thickness is reduced to a few
147 nanometers dramatically reduces the chances of developing RAF, even when the temperature
148 selected for isothermal crystallization does not necessarily favor phase decoupling.
149 This work aims at (1) using FSC to estimate the equilibrium enthalpy of melting of several
150 crystallizable polymers, such as poly(ethylene terephthalate) (PET), poly(L-lactic acid)

(PLLA), poly(phenylene sulfide) (PPS), poly(ethylene 2,5-furandicarboxylate) (PEF) and poly(butylene 2,5-furandicarboxylate) (PBF), and (2) discussing the results in comparison with the literature and the most common method that uses DSC cross-compared with XRD.

2. MATERIALS AND METHODS

2.1 Materials

Commercial grades of poly(ethylene terephthalate) (PET), poly(L-lactic acid) (PLLA) and poly(phenylene sulfide) (PPS) were purchased in the form of pellets, with the exception of PET that was purchased as a film. Poly(ethylene 2,5-furandicarboxylate) (PEF) and poly(butylene 2,5-furandicarboxylate) (PBF) were synthesized in the laboratories of the Wageningen Food and Biobased Research (FBR), The Netherlands. PEF was synthesized according to the procedure reported in [2]. PBF was obtained by melt polymerization of dimethyl-furan-dicarboxylic acid (DMFDCA) with 1,4-butanediol using $Ti(O\text{-}i\text{-}Pr)_4$ as a catalyst. The synthesized polymer was subjected to solid-state post-condensation (SSPC) and then used without further purification. All the samples were dried prior to measurement: PET and PLLA were dried at T_g + 10°C for at least 4h, whereas PPS, PEF and PBF were stored in a desiccator with P_2O_5 for at least 24h. The list of samples used in this study is reported in Table 2. Nanoscale samples were crystallized *in situ* on Fast Scanning Calorimetry (FSC) sensors and subsequently characterized by FSC. Bulk samples were crystallized in an oven and then characterized by wide-angle X-Ray Diffractometry (XRD), Differential Scanning Calorimetry (DSC), Modulated-Temperature DSC (MT-DSC) and FSC.

Table 2 List of samples along with their number-average molecular weight ($\overline{M_n}$), weight-average molecular weight ($\overline{M_w}$), polydispersity index ($\overline{M_w}/\overline{M_n}$), grade and source.

Sample	$\overline{M_n}$ [g·mol^{-1}]	$\overline{M_w}$ [g·mol^{-1}]	$\overline{M_w}/\overline{M_n}$	Grade, Source
PET	31 000	62 000	2.00	Carolex, France
PLLA	53 000	97 000	1.80	PLI005, Natureplast, France
PPS	n.a.	n.a.	n.a.	FORTRON 0214, Celanese, France
PEF	11 500	18 000	1.60	Wageningen FBR, The Netherlands
PBF	36 000	74 500	2.07	Wageningen FBR, The Netherlands

2.2 Fast Scanning Calorimetry (FSC)

FSC measurements were performed using a Flash-DSC 1 calorimeter (Mettler-Toledo) equipped with a HUBER TC100 intracooler. Prior to use, each MultiSTAR UFS 1 MEMS empty chip was conditioned and corrected according to the manufacturer's procedure. Temperature calibration was performed according to the procedures reported in the literature [84]. The dynamic thermal lag corresponds to half the distance between the glass transition temperatures measured at the same heating and cooling rates; the static thermal lag corresponds to a third of the distance between the onset melting temperatures of two indium samples, one placed on top of the polymer sample and the other directly placed on the reference [85]. The dynamic thermal lag ΔT_D (which depends on the selected heating and cooling rates) was measured at $\beta^+ = |\beta^-| = 1000$ K·s^{-1} and found to be less than 4K. As for the static thermal lag ΔT_S (which mostly depends on the sample thickness), values less than 2K were ensured by preparing samples with thickness of 10 ± 3 µm, as recommended by Toda et al. [83] to prevent thermal gradients, and in agreement with the findings previously reported in the literature for different polymers [86-88]. The thickness of the samples was estimated from the determined mass, the literature value of density, and the area measured by optical microscopy, as previously done by Toda et al. [83]. A constant nitrogen flow of 20 mL·min^{-1} was used to purge the measurement cell. Prior to *in situ* crystallization, the samples were quenched to their reference amorphous state by performing five heating/cooling steps at a rate

of 1000 K·s^{-1} over a temperature range going from -60°C to the melt in order to ensure that any previous thermo-mechanical history was erased. The mass of the FSC samples used for this study ranged between 27 and 251 ng. The mass values were estimated using equation (2):

$$m = \Delta C_{p_{am}}^{FSC}\,[J\cdot K^{-1}]/\Delta C_{p_{am}}^{MT-DSC}[J\cdot g^{-1}\cdot K^{-1}] \qquad (2)$$

Where $\Delta C_{p_{am}}^{FSC}\,[J\cdot K^{-1}]$ is the heat capacity step at the glass transition estimated from FSC curves (β^+ = 1000 K·s^{-1}) and $\Delta C_{p_{am}}^{MT-DSC}[J\cdot g^{-1}\cdot K^{-1}]$ is the heat capacity step at the glass transition obtained by a MT-DSC scan of the quenched reference bulk samples (heating rate β^+ = 2 K·min^{-1} ≈ 0.033 K·s^{-1}).

2.3 Modulated-Temperature Differential Scanning Calorimetry (MT-DSC)

MT-DSC measurements were carried out on a DSC Q100 (TA Instruments) using the Tzero technology. Temperature, energy and heat capacity calibrations were performed with indium and sapphire standards. All the thermal treatments and characterizations were done under a constant nitrogen flow of 50 mL·min^{-1} to prevent any oxidative degradation of the samples. The mass of MT-DSC bulk samples ranged between 5 and 10 mg. The modulated-temperature heating ramps were designed using a heat-only protocol, starting from -70°C and reaching a temperature that ensures the complete melting of each sample, with a heating rate of 2 K·min^{-1}, a modulating amplitude of ± 0.318K and a period of 60s, as recommended in [89], to prevent reversible crystallization during melting. MT-DSC was used to determine the heat capacity step at the glass transition for the quenched bulk samples $\Delta C_{p_{am}}^{MT-DSC}[J\cdot g^{-1}\cdot K^{-1}]$, which is further needed to estimate the mass of FSC nanoscale samples according to equation (2).

2.4 Differential Scanning Calorimetry (DSC)

DSC measurements were made on a DSC TA2920 (TA Instruments). Energy and temperature calibrations were carried out using an indium standard. All the characterizations were done after ballistic cooling to -20°C, with a heating rate of 20 K·min^{-1} under a constant nitrogen flow of 50 mL·min^{-1} to prevent any oxidative degradation of the samples. The mass of DSC bulk samples ranged between 5 and 10 mg. DSC was used to estimate the enthalpy of melting ΔH_m of bulk samples to be used in equation (1).

2.5 Wide-angle X-Ray Diffractometry (XRD)

XRD spectra were recorded at room temperature on (16 mm x 16 mm) samples by a Bruker D8 X-ray diffractometer in the angular range 2θ = 5-40°, with a step of 0.05° and a counting time of 1s/step, using a Co Kα radiation (λ = 2.29Å). The patterns were obtained by subtracting the background signal and averaging at least three spectra recorded on the same spot of the sample. XRD patterns were then exploited with different fitting methods (multi-peak fitting with Gaussian or Pearson functions) by two different operators to have an estimation of the uncertainties on the calculation of the apparent degree of crystallinity X_c^{XRD}. This value was determined as a ratio of areas, i.e. the area corresponding to the crystalline peaks divided by the total area of the pattern (crystalline peaks plus amorphous halo), and used in equation (1).

2.6 Sample preparation and thermal treatments

In order to create a microstructure with a reduced amount of RAF, nanoscale samples were crystallized *in situ* on FSC sensors using selected conditions of temperature and time.

2.6.1 Choice of the crystallization temperature T_c

The samples were melted, cooled down to a temperature within the crystallization temperature range, held in isothermal conditions for a constant crystallization time (60 minutes), cooled down to -60°C with a cooling rate of 1000 $K \cdot s^{-1}$ (the same rate used for measurements), and then heated again to observe the melting endotherm. This protocol was repeated at progressively increasing temperatures (the increase was done by steps of 5°C) and the crystallization temperature T_c was selected as the highest temperature at which the crystallization induction time was shorter than the isothermal time (i.e. crystallization started within a time ≤60 minutes). The choice of 60 minutes results from a compromise between a reasonable crystallization time and a sufficiently high crystallization temperature for crystal perfection.

2.6.2 Preparation of maximum crystallized nanoscale samples

A cycle of isothermal crystallizations was performed on each sample at the selected temperature T_c for progressively increasing durations until a microstructure was formed that showed no further increase in the melting peak, i.e. until the crystallinity degree reached its maximum. The corresponding time was taken as t_c^{max}.

2.6.3 Preparation of maximum crystallized bulk samples to be compared to nanoscale samples

The results obtained by FSC on nanoscale samples were compared to the results obtained by more conventional techniques (XRD, DSC and MT-DSC), which require bigger samples. To this purpose, semi-crystalline bulk samples were also prepared by melting the polymer samples between two Teflon sheets, then quickly transferring the assembly to an oven previously set at the selected crystallization temperature T_c and holding the isothermal conditions for a crystallization time at least equal to t_c^{max}. Maximum crystallized bulk samples were obtained by holding the selected crystallization temperature T_c for a crystallization time

varying between 2 and 5h. The fully amorphous counterparts were obtained by melting the samples between two Teflon sheets, followed by quenching in cold water.

2.7 Determination of the equilibrium enthalpy of melting (ΔH_m^0)

Equation (1) gives a good estimate of ΔH_m^0 only if the same microstructure can be obtained by two different techniques (e.g. DSC and XRD) and the corresponding results (i.e. ΔH_m^{DSC} and X_C^{XRD}) are available for cross-comparison. With the value of ΔH_m^0, the degree of crystallinity X_c of a semi-crystalline polymer can be determined by performing a single DSC run and applying the following equation [90, 91]:

$$X_c = \Delta H_m^{DSC} / \Delta H_m^0 \quad (3)$$

Where ΔH_m^{DSC} is the enthalpy of melting obtained by integration of the melting endothermic peak. Cebe et al. [8] recently applied equation (1) to FSC experiences and rewrote it as follows:

$$\Delta H_m^{FSC}(T_m)[J] = \Delta H_m^0(T_m)[J \cdot g^{-1}] * (mass\ [g] * X_c) \quad (4)$$

With X_c obtained either by combining FSC results with information found in the literature (i.e. the heat of fusion of 100% crystal at T_m and the specific heat capacity at a given temperature, judiciously chosen) [8] and/or by a different experimental technique (through independent measurements performed on similarly treated samples – under the assumption that uniform thermal treatment would result in uniform crystallinity, whatever the size of the sample and the experimental technique).

According to equation (4), the value of ΔH_m^0 can be determined if the sample mass, degree of crystallinity and enthalpy of melting are known, i.e. ΔH_m^0 can be directly deduced from the slope of a plot representing the enthalpy of melting ΔH_m^{FSC} as a function of $(mass[g] * X_c)$. When the conditions for a two-phase model are fulfilled, the degree of crystallinity X_c can be directly estimated from the ratio between the heat capacity change at the glass transition of a

crystallized sample ($\Delta C_{p_{cryst}}$) and the value previously found for its fully amorphous counterpart ($\Delta C_{p_{am}}$) as follows:

$$X_c^{2ph} = 1 - (\Delta C_{p_{cryst}} / \Delta C_{p_{am}}) \quad (5)$$

If the works of Cebe et al. [8] (using FSC) and Pyda et al. [26, 56] (correlating the enthalpy of melting and the heat capacity change at the glass transition in two-phase microstructures) are merged, equations (1), (4) and (5) can be combined as:

$$\Delta H_m^{FSC}(T_m)[J \cdot g^{-1}] = -(\Delta H_m^0(T_m)[J \cdot g^{-1}] / \Delta C_p{}_{am}^{FSC} [J \cdot g^{-1} \cdot K^{-1}]) * \Delta C_p{}_{cryst}^{FSC} [J \cdot g^{-1} \cdot K^{-1}] + \Delta H_m^0(T_m) [J \cdot g^{-1}] \quad (6)$$

ΔH_m^0 can therefore be calculated from the intercept of a plot representing the enthalpy of melting $\Delta H_m^{FSC}(T_m)[J \cdot g^{-1}]$ versus the heat capacity step at the glass transition $\Delta C_p{}_{cryst}^{FSC}[J \cdot g^{-1} \cdot K^{-1}]$. ΔH_m^{FSC} is obtained by integrating the endothermic peak observed on the FSC curves normalized to the sample mass (according to equation (2)) with a linear baseline going from the end of the glass transition up to the melt. $\Delta C_p{}_{cryst}^{FSC}$ is obtained by extrapolating the baselines of the FSC curves in the glassy/solid state ($T<T_g$) and in the liquid state ($T>T_g$) through the glass transition T_g (read as the midpoint of the heat capacity step), and calculating the difference between $baseline_{liquid}^{FSC}\big|_{T=Tg}$ and $baseline_{solid}^{FSC}\big|_{T=Tg}$. Values equivalent to a change in the heat capacity are obtained from the values of heat flow [mW] by conversion to [J] and normalization to the sample mass [g].

3. RESULTS AND DISCUSSION

Figure 1 shows the FSC curves recorded on nanoscale samples upon heating at β^+ = 1000 K·s^{-1} after *in situ* isothermal crystallization from the melt at the crystallization temperature T_c during different crystallization times t_c followed by cooling down to -60°C at β^- = 1000 K·s^{-1}. Some of the samples investigated in this study are known to be potentially subjected to the

formation of a metastable crystalline phase (PLLA [1, 92], PEF [34, 93] and PBF [94]). A special care was given to the selection of T_c so that only the most stable crystalline phase was formed. In the case of PLLA, for instance, the crystallization from the melt at temperatures higher than 130°C leads to the formation of α crystals (helical chain segments aligned in an orthorhombic unit cell), whereas at temperatures lower than 100°C the formation of conformationally disordered α' crystals is observed [1]. The presence of metastable crystalline phases increases the risk of crystalline reorganization, which in turn affects the calculation of the enthalpy of melting. For this reason, PLLA samples were crystallized at T_c = 145°C. For similar reasons, T_c was set at 175°C in the case of PEF and 135°C in the case of PBF (whose thresholds between different crystalline phases were found at 170°C [93] and 130°C [94], respectively).

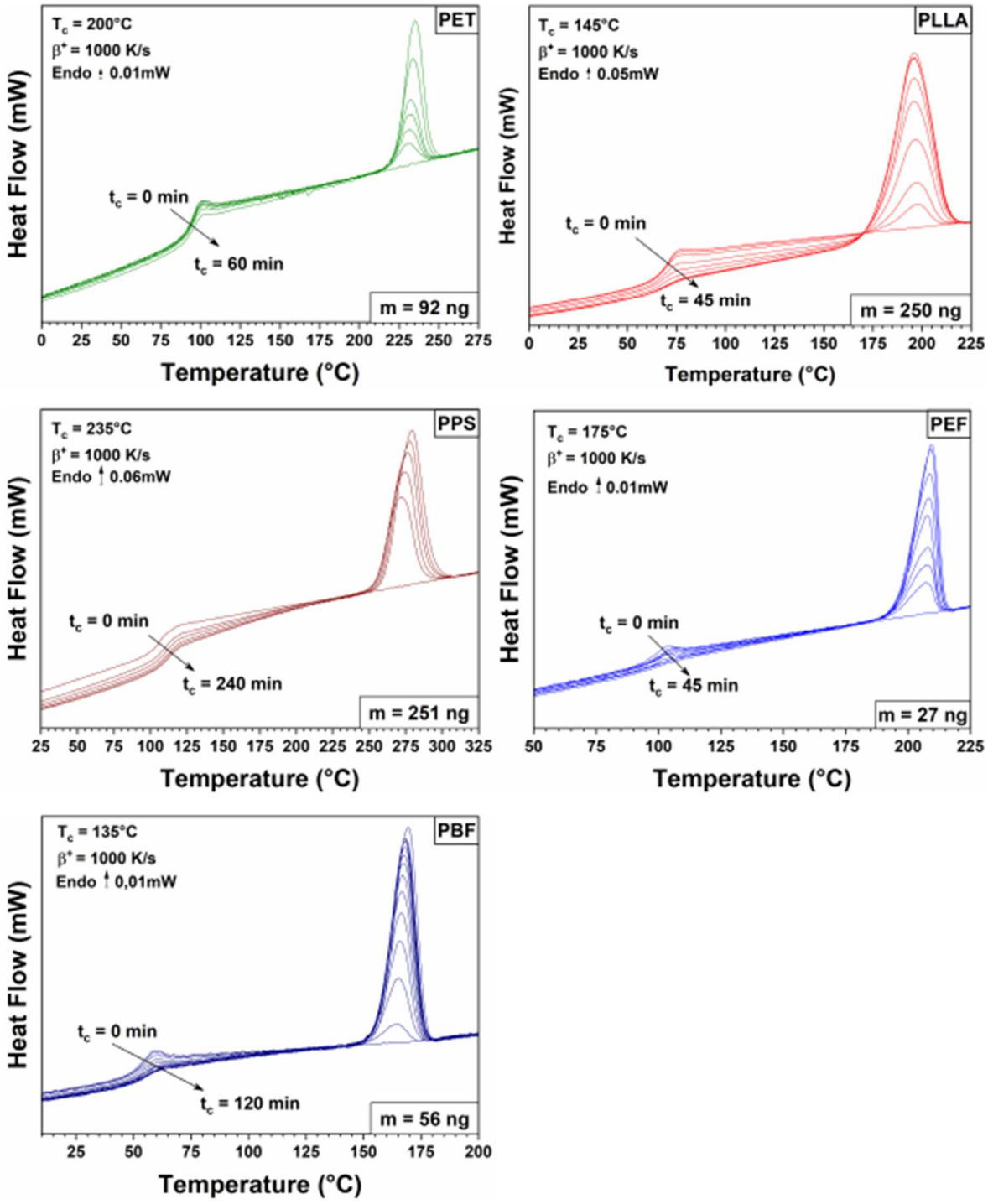

Figure 1 FSC curves recorded upon heating at $\beta^+ = 1000\ K \cdot s^{-1}$ on nanoscale samples of PET, PLLA, PPS, PEF and PBF after *in situ* isothermal crystallization from the melt at the crystallization temperature T_c during different crystallization times t_c.

The first encouraging evidence is that in Figure 1 all the samples show a single and relatively sharp melting peak, excluding the possibility of a melting/recrystallization process during

heating, which would have been typical of polymorphism or crystalline reorganization and is usually revealed by an exothermic signal partially or entirely overlapping the melting endotherm (as observed, for instance, in PLA [95-98]). As the crystallization time increases, the intensity of the melting endotherm increases. Since no cold crystallization occurs during the heating ramp, the values of ΔH_m^{FSC} obtained by integrating the endothermic peaks in Figure 1 can be reliably and exclusively associated to the melting of the crystalline domains progressively created during the previous isothermal treatments. For some polymers (e.g. for PET and PPS), the maximum of the melting endotherm slightly shifts to higher temperatures as the crystallization time increases, suggesting that the crystallization progresses and the crystalline lamellae grow thicker, in agreement with the Gibbs-Thomson equation [99].

One may also note that the baseline of the FSC curves in Figure 1 slightly changes as the crystallinity of the samples increases. This dependence is observed in the solid state (from the glassy state up to the onset of melting) but never observed in the molten state, and is particularly visible when the sample mass is relatively large (e.g. for PLLA and PPS). These changes may be due to some interfacial effects associated with stress transfers between the polymer sample and the SiN membrane of the sensor. Stress transfers could be the consequence of a mismatch in the thermal conductivity of the polymer sample and the SiN membrane of the sensor, but also to the shrinkage related to crystallization. The second hypothesis is most likely because the shrinkage of a polymer sample is expected to be proportional to the extent of crystallization, proportional to the sample mass and only visible when the sample is semi-crystalline (in the molten state the polymer is supposed to relax). These effects are not due to a sample mass change, because precautions were taken to make sure that the mass of polymer in contact with the sensor remained constant during the whole experimental protocol.

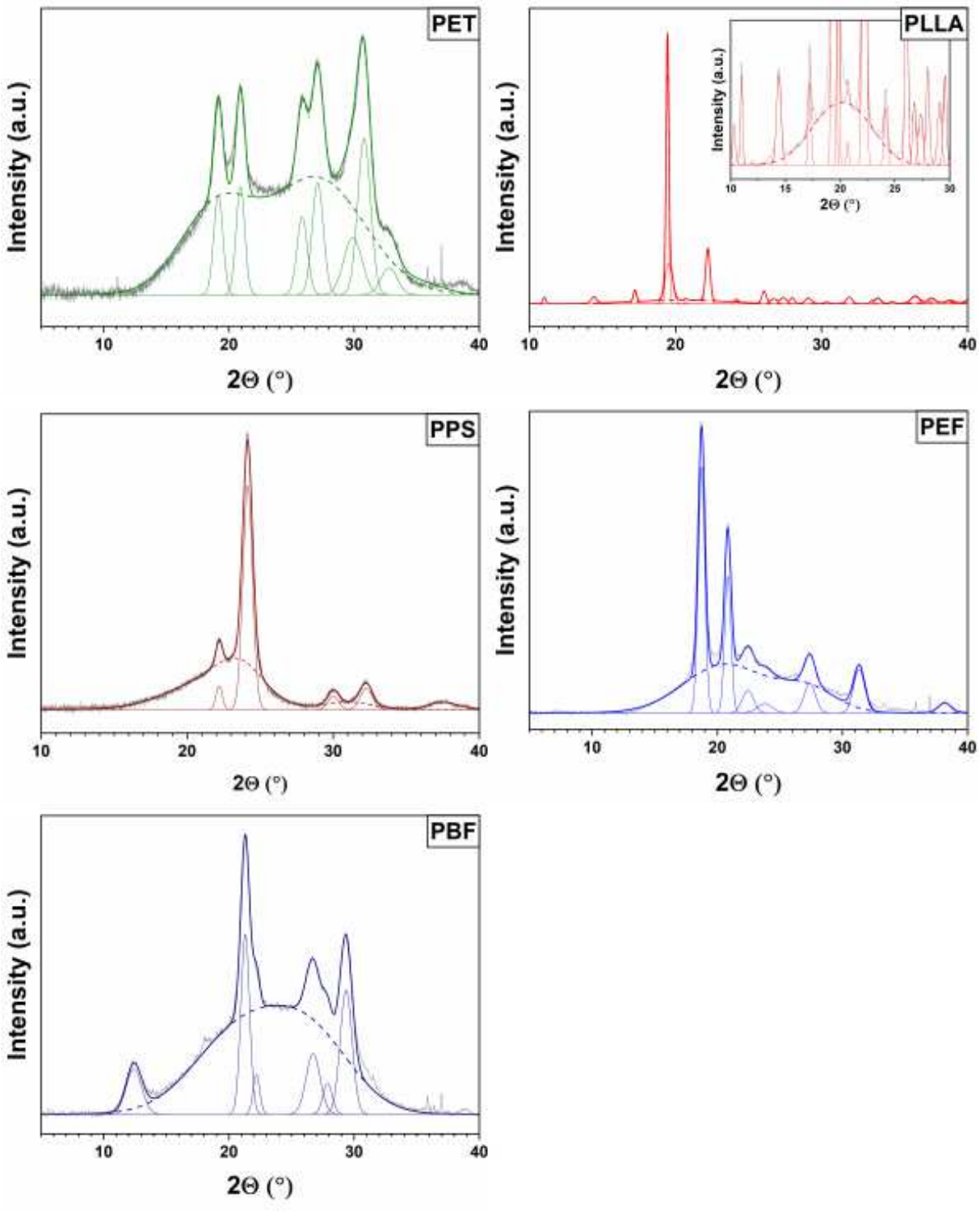

Figure 2 XRD patterns recorded at room temperature on maximum crystallized bulk samples of PET, PLLA, PPS, PEF and PBF after isothermal crystallization from the melt at the crystallization temperature T_c (solid lines). The raw data are in grey. The thick solid lines represent the fitting result. Thinner solid and dashed lines are also reported to represent the crystalline and amorphous contributions to each pattern (multi-peak fitting with Gaussian functions). The amorphous halos were fitted by two Gaussian peaks; the dashed lines

represent the sum of the peaks used for fitting. In the case of PLLA, an inset with suitable rescaling is provided to better visualize the amorphous halo.

XRD scans were recorded on maximum crystallized bulk samples to confirm that the crystalline phases grown during the isothermal crystallization at T_c are the most stable ones (Figure 2), which is consistent with the information previously reported in the literature about PLA [1, 92], PEF [34] and PBF [94]. The XRD patterns in Figure 2 were also used to estimate the apparent degree of crystallinity [100], a method that requires a careful subtraction of the amorphous halo. In this work, all the samples maximum crystallized in the bulk showed a complex amorphous halo that required two Gaussian peaks for fitting. Huo et al. [77] have already pointed out that the presence of RAF affects XRD patterns; being part of the amorphous phase, the RAF is expected to be included in the amorphous halo along with the MAF. The literature reports that the amorphous halo of PET can be deconvoluted in two Gaussian contributions [101]: the first one attributed to the interchain distances perpendicular to the plans of aligned aromatic rings, the second one attributed to the interchain distances within the plane of the aligned aromatics rings. Similarly to PET, two Gaussian contributions were used to deconvolute the amorphous halos of PLLA and PPS according to information reported in the literature [102, 103]. As for PEF and PBF, two Gaussian contributions were also used, even if no information is reported in the literature.

Figure 3 shows the values of the enthalpy of melting ΔH_m^{FSC} plotted against the values of the heat capacity step at the glass transition in the semi-crystalline samples $\Delta C_p{}_{cryst}^{FSC}$, both measured on the FSC curves reported in Figure 1.

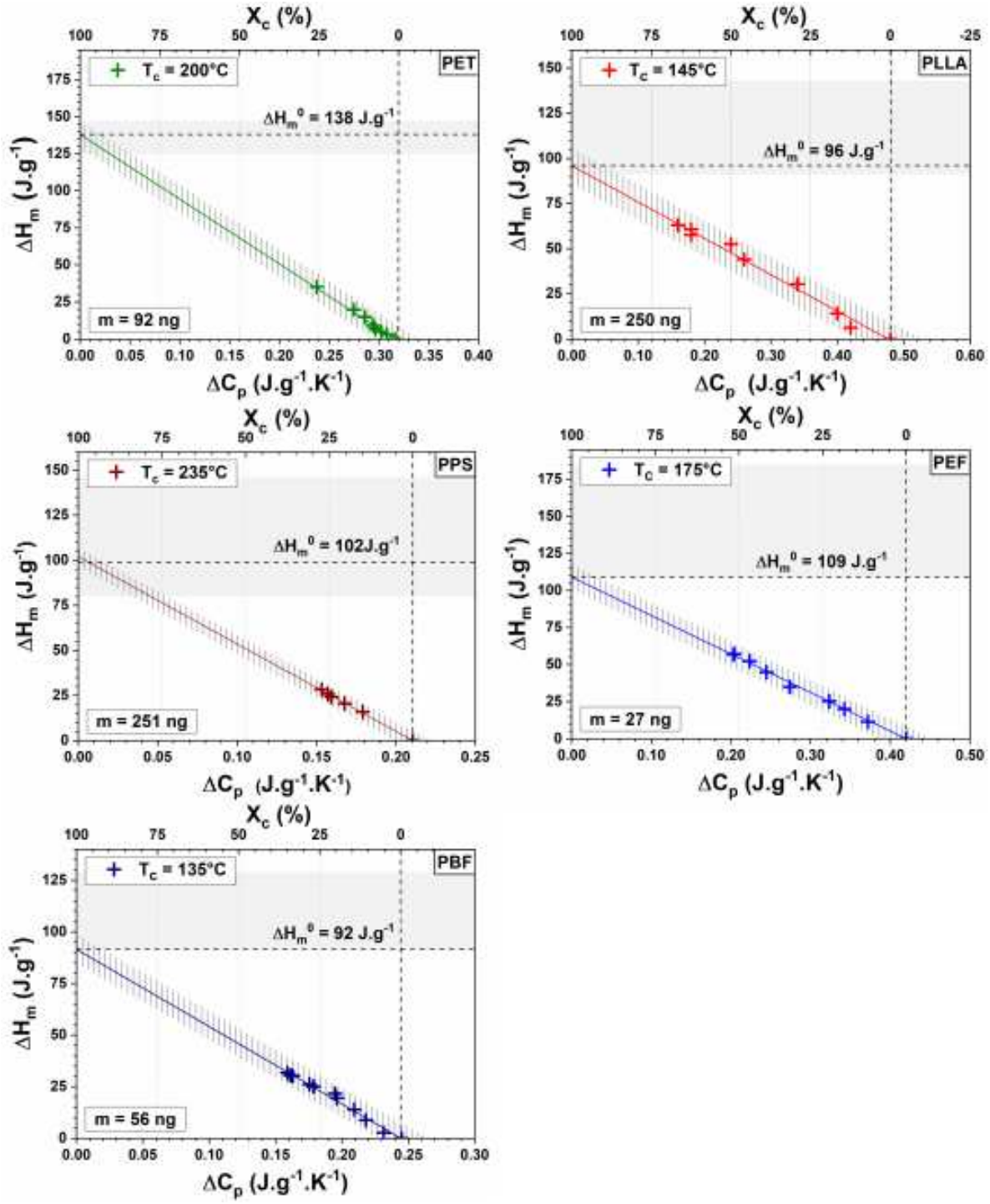

391

392 **Figure 3** Enthalpy of melting vs. heat capacity change at the glass transition obtained from
393 FSC curves normalized to the sample mass and the heating rate (Figure 1) for nanoscale
394 samples of PET, PLLA, PPS, PEF and PBF crystallized *in situ* at the crystallization
395 temperature T_c for different crystallization times t_c. The linear regression of the experimental
396 data (solid lines) extrapolated to $X_c = 100\%$ and $\Delta C_p = 0$ J·g^{-1}·K^{-1} reveals the equilibrium
397 enthalpy of melting ΔH_m^0 under the assumption of a two-phase model. The grey hatched areas
398 around the solid lines represent the uncertainty of ± 5% on the estimation of the apparent

399 degree of crystallinity. The grey horizontal areas represent the domain covered by the values
400 of ΔH_m^0 that can be found in the literature (Table 1) plus the values obtained in this work.
401
402 According to its definition, ΔH_m^0 could be straightforwardly calculated with the datasets
403 reported in Figure 3, provided that the hypothesis of a two-phase microstructure is verified.
404 Indeed, the comparison between the values of ΔH_m (with respect to its reference ΔH_m^0) and
405 $\Delta C_{p_{cryst}}$ (with respect to its reference $\Delta C_{p_{am}}$) obtained from the same DSC curve is generally
406 used to discuss the pertinence of a two-phase model to describe the microstructure of semi-
407 crystalline polymers. Whenever a discrepancy is revealed in the information provided by ΔH_m
408 (crystalline fraction X_c calculated according to equation (3)) and $\Delta C_{p_{cryst}}$ (residual
409 amorphous fraction relaxing at the glass transition), a three-phase model is adopted in the
410 place of equation (5) and the RAF is introduced to solve the discrepancy.

411 $$1 = X_c^{3ph} + (\Delta C_{p_{cryst}} / \Delta C_{p_{am}}) + X_{RAF} \qquad (7)$$

412 Nassar et al. [74] recently reported that growing crystals in a nanoscale confined environment
413 reduces the development of RAF, even when the temperature conditions are supposed to favor
414 the connections between the crystalline domains and the surrounding amorphous phase. The
415 samples used in FSC experiments are intrinsically nanoscale (the biggest weighs 250 ng),
416 which may eventually help limiting the formation of RAF for similar reasons, i.e. for a sort of
417 finite-size effect. With this being said, the choice of a two-phase model to determine the
418 degree of crystallinity using equation (5) applied to FSC curves sounds encouraging. Besides,
419 the experimental conditions used in this study for crystallization were designed to minimize
420 the development of RAF, and the fact that the baselines of the FSC curves in Figure 1 look
421 quite straight in the temperature range between the glass transition and the melt, suggests that
422 a two-phase model could actually apply to all the semi-crystalline microstructures obtained by
423 *in situ* isothermal crystallization on nanoscale samples. The literature reports that the amount

of RAF formed during the crystallization process typically decreases as the size and thermal stability of the crystalline phase increases [60], and it is well known that the size and thermal stability of the crystalline lamellae increases with the crystallization temperature [104]. The literature also reports that the development of RAF is typically associated to an increase in the glass transition temperature (revealing a mobility restriction of the RAF on the MAF) [105], as well as a modification of its shape (due to a different distribution of the relaxation times, revealing a stronger coupling between phases) [55]. These modifications of the glass transition, especially when associated to the development of irregular crystalline domains melting over an extended temperature range, would make it impossible to distinguish the microstructural information conveyed by the heat capacity change as a function of temperature (baseline) and the melting endotherm, respectively. None of these modifications were observed in the FSC curves recorded for this study.

When equation (6) is used to fit the data in Figure 3, the linear regression gives a slope that corresponds to $\Delta H_m^0(T_m)\ [J \cdot g^{-1}]/\Delta C_{p_{am}}^{FSC}\ [J \cdot g^{-1} \cdot K^{-1}]$ and an intercept that directly provides the value of ΔH_m^0. The dispersion of the experimental values around the linear fit (grey hatched areas in Figure 3) corresponds to ± 5 % uncertainty on the estimation of the degree of crystallinity. If this uncertainty were introduced in the calculation, the value of ΔH_m^0 would be affected by an uncertainty of ± 10 $J \cdot g^{-1}$ (which is acceptable when compared to the error introduced by a wrong estimation of the enthalpy of melting, e.g. in the case of crystalline reorganization during DSC measurement ramps at conventional heating rates). Indeed, there are several possible sources of uncertainties, and the scattering in the values of ΔH_m^0 found in the literature is quite explicit, as illustrated by the grey horizontal areas in Figure 3 covering all the values previously reported in Table 1. One of the main sources of uncertainty in determining the equilibrium enthalpy of melting by this method, is due to the fact that this is an extrapolative method. It is quite difficult to obtain a polymer with a highly

crystalline microstructure for which the two-phase assumption can be assuredly made. Most of the polymers investigated in this paper have a degree of crystallinity that barely reaches 30%. For these polymers, the uncertainty associated with the slope of the ΔH_m vs ΔC_p plots is much relevant. This being said, the values of ΔH_m^0 obtained in this study fall in the same range as the values previously reported in the literature by several authors, as illustrated by the grey areas in Figure 3. In the case of PET, for instance, for which no substantial divergences are found in the literature, the FSC protocol provides a value of 138 J·g^{-1}, which is in agreement with the value previously obtained by Wunderlich and Androsch (140 J·g^{-1}) [21, 60]. As a consequence, when it comes to relatively new polymers for which no data are found in the literature, such as PEF and PBF, one may assume that this method provides at least a preliminary estimation of ΔH_m^0 that is fairly reliable, yet debatable if different values are successively found by other experimental techniques. Table 3 summarizes the experimental conditions used for the *in situ* isothermal crystallization performed on the FSC sensors, as well as the main outcomes of the crystallization process measured by FSC on the maximum crystallized nanoscale samples (exploitation of Figure 1) and the corresponding values of ΔH_m^0.

Table 3 Crystallization temperature (T_c) and crystallization time (t_c^{max}) selected to reach the maximum crystallinity degree during *in situ* isothermal crystallization aiming to reduce coupling between phases. T_g and T_m are the glass transition temperature and the melting temperature of the maximum crystallized nanoscale samples measured by FSC. The equilibrium enthalpy of melting ΔH_m^0 was obtained according to equation (6) based exclusively on FSC results. For comparison's purposes, the crystallinities of maximum crystallized bulk and nanoscale samples, which were obtained by XRD and FSC respectively, are also reported ($X_{C\,max}^{XRD}$and $X_{C\,max}^{FSC}$).

Sample	T_c [°C]	t_c^{max} [min]	T_g [± 1 °C]	T_m [± 1 °C]	ΔH_m^0 [± 10 J·g^{-1}]	$X_{C\,max}^{XRD}$ [± 5%]	$X_{C\,max}^{FSC}$ [± 5%]
PET	200	60	92	235	138	37	25
PLLA	145	45	68	196	96	82	67
PPS	235	240	108	279	102	39	27
PEF	175	45	96	210	109	52	52
PBF	135	120	51	169	92	33	30

The experimental procedure proposed in this work can be compared to the ones commonly found in the literature that are based on the cross-comparison of two different techniques. PET is a good example to illustrate the possible sources of uncertainty when different methods are used to estimate ΔH_m^0. The XRD patterns recorded on maximum crystallized bulk samples (Figure 2) were used to calculate the apparent degree of crystallinity $X_{C\,max}^{XRD}$. The value obtained for PET is 37 ± 5%. Ruland method (based on the conservation of the total scattered intensity by a set of atoms, independent on their structural order) could have been used to obtain the absolute degree of crystallinity [100], but most of the works reported in the literature use the method based on the ratio of areas. When equation (1) is used to cross-compare $X_{C\,max}^{XRD}$ with the enthalpy of melting measured by conventional DSC, a value of 162 J·g^{-1} is obtained. When FSC results are used instead of DSC in equation (1), the cross-comparison with $X_{C\,max}^{XRD}$ provides a value of 165 J·g^{-1}. These values are quite different with respect to the values found in the literature (140 J·g^{-1} [21], 125 J·g^{-1} [22], Table 1), independently on the technique used to measure the enthalpy of melting. The value obtained by the FSC method is much closer to the values of the literature (138 J·g^{-1}). Comparing different values of ΔH_m^0 is definitely a multifactor problem that requires a deeper understanding of both the advantages and drawbacks of the experimental procedures used to obtain them. The differences may be acceptable or very large, depending on the nature of the sample (some polymers crystallize faster, easier and more regularly than other polymers, generating different amounts of RAF), on the design of the experimental protocol used for

crystallization (which includes the size of the sample and the crystallization conditions, i.e. the crystallization temperature and time), as well as on the calculation procedure. Since ΔH_m^0 is estimated by extrapolating the experimental data (crystallinity degree X_c vs. enthalpy of melting ΔH_m) obtained on samples with different crystallinity degrees, it is mandatory to ensure the accuracy on the calculation of these quantities. In general, techniques such as XRD and DSC are used to cross-compare the results obtained on bulk samples crystallized in controlled conditions. Bulk samples are subjected to bigger thermal gradients, resulting in less controlled crystallization conditions and less regular microstructures. Besides, using conventional DSC to determine the enthalpy of melting of semi-crystalline polymers expands the level of uncertainty because of crystalline reorganization that is sometimes observed during the heating ramps, and that is hardly distinguished from the baseline drift related to the devitrification of the RAF. Using FSC improves the accuracy of measurement thanks to the extremely fast heating rates, which exclude any possible crystalline reorganization and suppress the effects eventually due to polymorphism. Last but not least, in suitable and controlled crystallization conditions, FSC allows the concomitant measurement of $X_{MAF} = 1 - X_C$ and ΔH_m, considerably reducing the uncertainties due to the cross-comparison of samples whose microstructures are not necessarily the same because of sampling heterogeneities. The main source of uncertainty for the FSC method proposed here is related to the fact that ΔH_m^0 is estimated under the assumption that a two-phase microstructure is obtained during the *in situ* crystallization protocol. For this reason, an accurate selection of the crystallization temperature T_c should be done with the purpose of growing regular crystalline domains with reduced connections between phases, i.e. with a negligible amount of RAF.

Among the samples shown in Figure 1, PLLA and PPS are the ones with the largest masses (~250 ng). Sample mass and crystallization temperature are two parameters that possibly

affect the results of FSC measurements and the following data treatment. However, it is quite difficult to distinguish how these parameters respectively contribute to the combined uncertainty on ΔH_m^0 because it is very hard to prepare several FSC sensors with samples having exactly the same mass and shape, and placed exactly in the same position on the membrane. Figure 4 shows the results obtained on smaller samples of PLLA and PPS (58 ng and 94 ng respectively) at higher crystallization temperatures (149°C and 243°C respectively) with respect to Figure 1.

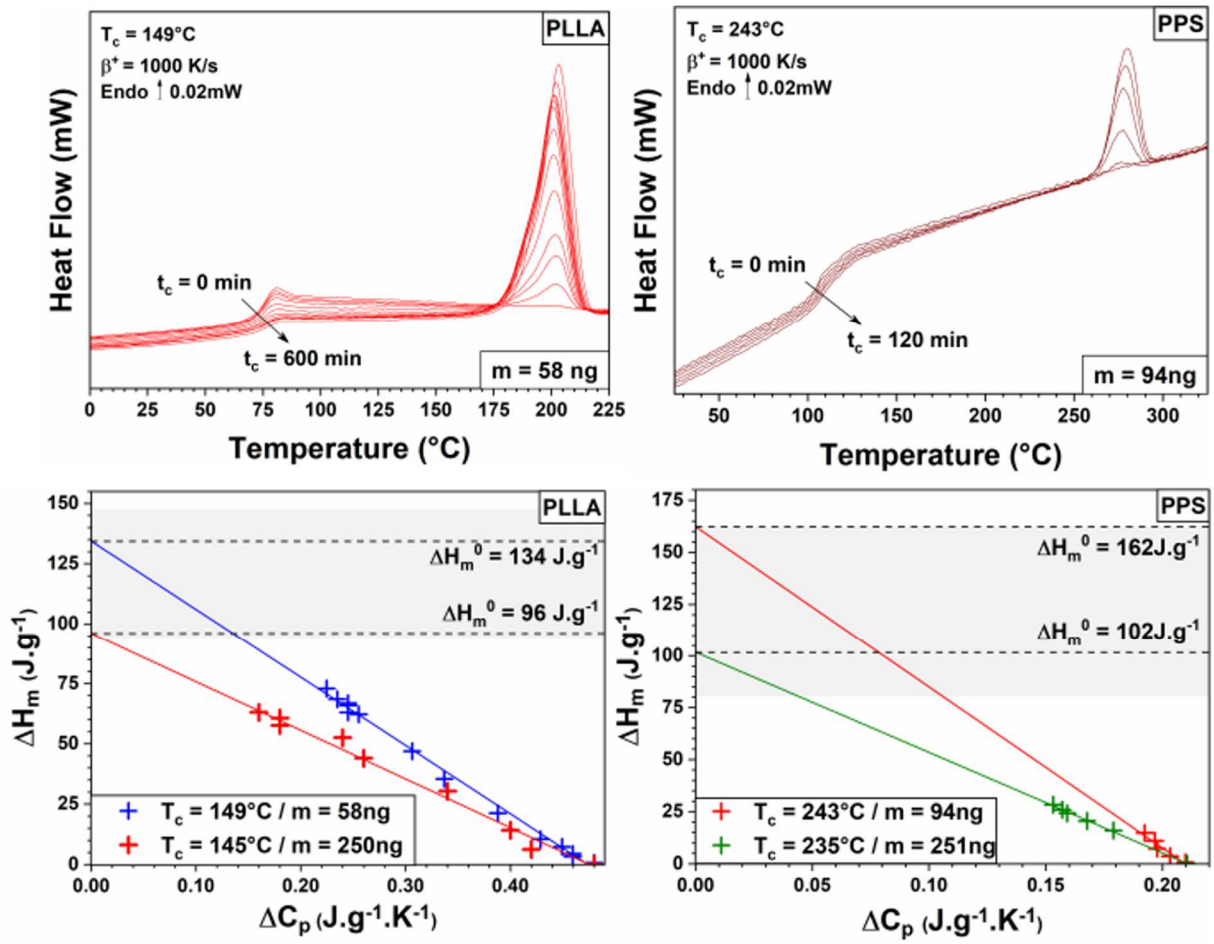

Figure 4 (top) FSC curves recorded upon heating at β^+ = 1000 K·s^{-1} on nanoscale samples of PLLA and PPS after *in situ* isothermal crystallization from the melt at two different crystallization temperatures (145°C and 149°C for PLLA, 235°C and 243°C for PPS) during different crystallization times. Smaller samples were used with respect to Figure 1 (58 ng vs. 250 ng for PLLA, 94 ng vs. 251 ng for PPS). **(bottom)** Enthalpy of melting vs. heat capacity change at the glass transition obtained from the FSC curves normalized to the sample mass

and to the heating rate. The linear regression (solid lines) of the experimental data (crosses) extrapolated to $X_c = 100\%$ and $\Delta C_p = 0$ J·g^{-1}·K^{-1} reveals the equilibrium enthalpy of melting ΔH_m^0 under the assumption of a two-phase model. The grey horizontal areas represent the domain covered by the values of ΔH_m^0 that can be found in the literature (Table 1) plus the values obtained in this work.

The ΔH_m vs ΔC_p plots reveal that, for these polymers, the extrapolated value of ΔH_m^0 is indeed quite dependent on the sample mass and/or on the choice of T_c. Further studies are required to evaluate the influence of these parameters. It should be reminded that all extrapolative methods have intrinsic limitations that are sources of uncertainties, and this is particularly true when the extrapolation is done on a large range of values starting with few points unevenly distributed (the case of PPS crystallized at 243°C is a good example). From this point of view, the extrapolation done on the basis of FSC measurements is neither better nor worse than any other extrapolative method, but provides values in agreement with the literature. Besides, there are polymers (such as PET) that are quite insensitive to the choice of a different crystallization temperature. The same PET sample was crystallized at three different temperatures (190°C, 200°C, and 210°C) and the values of ΔH_m^0 obtained (141 J·g^{-1}, 138 J·g^{-1} and 133 J·g^{-1} respectively) are quite similar and in perfect agreement with the literature (140 J·g^{-1} [21] and 125 J·g^{-1} [22]) (Figure 5).

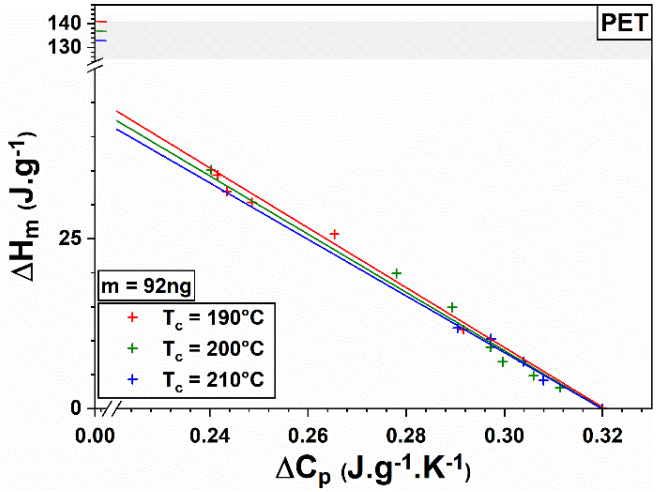

Figure 5 Extrapolation based on the FSC measurements on a nanoscale sample of PET (92 ng) isothermally crystallized from the melt at three different crystallization temperatures (190°C, 200°C and 210°C) during different crystallization times. The linear regression (solid lines) of the experimental data (crosses) extrapolated to $X_c = 100\%$ and $\Delta C_p = 0$ J·g^{-1}·K^{-1} provides a values of $\Delta H_m^0 = 137 \pm 4$ J·g^{-1}. The grey horizontal area represents the domain covered by the values of ΔH_m^0 found in the literature (Table 1).

Other samples may be more sensitive to the choice of T_c, especially if they have peculiar crystallization features such as polymorphism. PLLA, for instance, exhibits several types of crystal modifications (α, α′, β, and γ phases) that are sometimes difficult to isolate, even if the crystallization temperature is accurately selected. The ΔH_m vs ΔC_p plots reported in Figure 4 (bottom) suggest that PLLA is extremely sensitive to the choice of T_c. Table 3 reported a value of $\Delta H_m^0 = 96 \pm 10$ J·g^{-1} for PLLA crystallized at T_c = 145°C, but a much different value is obtained for T_c = 149°C ($\Delta H_m^0 = 134 \pm 10$ J·g^{-1}). None of these values is in disagreement with the literature, because Pyda et al. [26] and Kalish et al. [28] reported values of 91 J·g^{-1} (at T_c = 145°C) and 96 J·g^{-1} (at T_c = 150°C) respectively, whereas Miyata et al. [25] and Badrinarayanan et al. [27] reported values of 135 J·g^{-1} and 146 J·g^{-1} respectively; the most accurate approach seems to be the one proposed by Righetti et al. [1], which suggests to take into account the temperature dependence of ΔH_m^0.

These preliminary results indicate that polymers are not equally sensitive to parameters such as the sample mass and the crystallization temperature. As potential sources of uncertainty on the extrapolated value of the equilibrium enthalpy of melting, these parameters definitely deserve further investigations. As a perspective, it would also be interesting to measure the crystallinity degree by recording XRD patterns directly on the FSC sensor, according to the technical solutions proposed by Ivanov, Cavallo, Vlassak and their-coworkers [84, 98, 106, 107], who worked out some feasible solutions to combine XRD with FSC.

4. CONCLUSIONS

This work shows that the equilibrium enthalpy of melting ΔH_m^0 can be determined by fast scanning calorimetry (FSC), provided that suitable crystallization conditions are selected to reduce the connection between phases. The metrological concept relies, as usual, on the characterization of samples having microstructures with different degrees of crystallinity and the extrapolation of the experimental data to the theoretical situation of a 100% crystalline polymer. Contrarily to the methods commonly found in the literature, which are based on the cross-comparison of different experimental techniques (such as XRD and DSC) performed on different samples, this method is only calorimetric and significantly reduces the uncertainties related to (1) thermal gradients (FSC measurements are performed on nanoscale samples), (2) polymorphism and/or crystalline reorganization (FSC ramps are recorded at very high heating rates), and (3) sample heterogeneities (all the information required to calculate ΔH_m^0 is obtained from the same curve, recorded on the same sample). This method applies to any crystallizable polymer that is quenchable and for which a two-phase microstructure with a negligible amount of rigid amorphous fraction and reduced connections between phases is obtained under controlled crystallization conditions. The protocol of isothermal crystallization is performed *in situ* on nanoscale samples placed on the FSC sensor. The optimization of the crystallization parameters (temperature and time) should be preliminarily done according to the selected samples, especially for polymers that are subjected to polymorphism and/or particularly sensitive to the choice of the crystallization temperature. This method was used to estimate the equilibrium enthalpy of melting ΔH_m^0 of well-known polymers, such as PET and PPS, as well as of more recent biopolymers, such as PLLA, PEF and PBF.

606

607 **ACKNOWLEGMENTS**

608 The authors thank the Région Normandie and the European FEDER for their financial support
609 through the SCAMPI project (Aurélie Bourdet's PhD program) and the FARM Rin Recherche
610 project (Estève Ernault's post-doc position), as well as the French Ministère de
611 l'Enseignement Supérieur et de la Recherche for the financial support for Clément Fosse's
612 PhD program. The authors also thank Dr Benoît Vieille for providing PPS pellets.

613

614 **REFERENCES**

615 [1] M.C. Righetti, M. Gazzano, M.L. Di Lorenzo, R. Androsch. Enthalpy of melting of α′-
616 and α-crystals of poly(l-lactic acid). European Polymer Journal. 70 (2015) 215-220.
617 doi:10.1016/j.eurpolymj.2015.07.024.

618 [2] S. Thiyagarajan, W. Vogelzang, R.J.I. Knoop, A.E. Frissen, J. van Haverenab, D.S. van
619 Es. Biobased furandicarboxylic acids (FDCAs): effects of isomeric substitution on polyester
620 synthesis and properties. Green Chemistry. 16 (2014) 1957-1966. doi:10.1039/c3gc42184h.

621 [3] A. Bourdet, A. Esposito, S. Thiyagarajan, L. Delbreilh, F. Affouard, R.J.I. Knoop, E.
622 Dargent. Molecular Mobility in Amorphous Biobased Poly(ethylene 2,5-furandicarboxylate)
623 and Poly(ethylene 2,4-furandicarboxylate). Macromolecules. 51 (2018) 1937-1945.
624 doi:10.1021/acs.macromol.8b00108.

625 [4] R. Androsch, M. Soccio, N. Lotti, D. Cavallo, C. Schick. Cold-crystallization of
626 poly(butylene 2,6-naphthalate) following Ostwald's rule of stages. Thermochimica Acta. 670
627 (2018) 71-75. doi:10.1016/j.tca.2018.10.015.

628 [5] R. Chiang, P.J. Flory. Equilibrium between Crystalline and Amorphous Phases in
629 Polyethylene 1. Journal of the American Chemical Society. 83 (1961) 2857-2862.
630 doi:10.1021/ja01474a017.

631 [6] B. Wunderlich, C.M. Cormier. Heat of fusion of polyethylene. Journal of Polymer Science
632 Part A-2: Polymer Physics. 5 (1967) 987-988. doi:10.1002/pol.1967.160050514.

633 [7] C.M.L. Atkinson, M.J. Richardson. Thermodynamic properties of ideally crystalline
634 polyethylene. Transactions of the Faraday Society. 65 (1969) 1764.
635 doi:10.1039/tf9696501764.

636 [8] P. Cebe, D. Thomas, J. Merfeld, B.P. Partlow, D.L. Kaplan, R.G. Alamo, A. Wurm, E.
637 Zhuravlev, C. Schick. Heat of fusion of polymer crystals by fast scanning calorimetry.
638 Polymer. 126 (2017) 240-247. doi:10.1016/j.polymer.2017.08.042.

639 [9] F. Danusso, G. Gianotti. Fusion enthalpy and entropy of isotactic polypropylene.
640 European Polymer Journal. 4 (1968) 165-171. doi:10.1016/0014-3057(68)90018-9.

641 [10] R. Dedeurwaerder, J.F.M. Oth. Enthalpie et entropie de fusion du polystyrolène
642 isotactique. Journal de Chimie Physique. 56 (1959) 940-945. doi:10.1051/jcp/1959560940.

643 [11] I. Abu-Isa, M. Dole. Specific Heat of Synthetic High Polymers. XII. Atactic and Isotactic
644 Polystyrene 1. The Journal of Physical Chemistry. 69 (1965) 2668-2675.
645 doi:10.1021/j100892a031.

646 [12] G. Gee, Proceedings of the Chemical Society. London (1957) 111.

647 [13] J.R. Schaefgen. Estimation of the heat and entropy of fusion of some polyhydrocarbons.
648 Journal of Polymer Science. 38 (1959) 549-552. doi:10.1002/pol.1959.1203813427.

649 [14] S. Newman. On the characterization of stereoregular polymers. II. Polypropylene.
650 Journal of Polymer Science. 47 (1960) 111-137. doi:10.1002/pol.1960.1204714911.

651 [15] B. Ke. Characterization of polyolefins by differential thermal analysis. Journal of
652 Polymer Science. 42 (1960) 15-23. doi:10.1002/pol.1960.1204213903.

653 [16] R.W. Wilkinson, M. Dole. Specific heat of synthetic high polymers. X. Isotactic and
654 atactic polypropylene. Journal of Polymer Science. 58 (1962) 1089-1106.
655 doi:10.1002/pol.1962.1205816668.

656 [17] E. Passaglia, H.K. Kevorkian. Specific Heat of Atactic and Isotactic Polypropylene and
657 the Entropy of the Glass. Journal of Applied Physics. 34 (1963) 90-97.
658 doi:10.1063/1.1729095.

659 [18] J.G. Fatou. Melting temperature and enthalpy of isotactic polypropylene. European
660 Polymer Journal. 7 (1971) 1057-1064. doi:10.1016/0014-3057(71)90138-8.

661 [19] P. Marx, C.W. Smith, A.E. Worthington, M. Dole. Specific Heat of Synthetic High
662 Polymers. IV. Polycaprolactam. The Journal of Physical Chemistry. 59 (1955) 1015-1019.
663 doi:10.1021/j150532a005.

664 [20] S. Gogolewski, A. Pennings. Crystallization of polyamides under elevated pressure: 2.
665 Pressure-induced crystallization of nylon-6 (polycapramide) from the melt. Polymer. 16
666 (1975) 673-679. doi:10.1016/0032-3861(75)90075-0.

667 [21] M. Pyda (Ed.), ATHAS Data Bank.

668 [22] H.F. Mark et al. (Eds.). Encyclopedia of Polymer Science and Engineering. Vol 12, John
669 Wiley and Sons, New York, (1985), p. 226.

670 [23] A. Conix, R. Van Kerpel. Crystallization behavior and melting properties of m-
671 phenylene group containing polyesters. Journal of Polymer Science. 40 (1959) 521-532.
672 doi:10.1002/pol.1959.1204013720.

673 [24] K.-H. Illers. Heat of fusion and specific volume of poly(ethylene terephthalate) and
674 poly(butylene terephthalate. Colloid and Polymer Science. 258 (1980) 117-124.
675 doi:10.1007/BF01498267.

676 [25] T. Miyata, T. Masuko. Crystallization behaviour of poly(l-lactide). Polymer. 39 (1998)
677 5515-5521. doi:10.1016/S0032-3861(97)10203-8.

678 [26] M. Pyda, R.. Bopp, B. Wunderlich. Heat capacity of poly(lactic acid). The Journal of
679 Chemical Thermodynamics. 36 (2004) 731-742. doi:10.1016/j.jct.2004.05.003.

680 [27] P. Badrinarayanan, K.B. Dowdy, M.R. Kessler. A comparison of crystallization behavior
681 for melt and cold crystallized poly (l-Lactide) using rapid scanning rate calorimetry. Polymer.
682 51 (2010) 4611-4618. doi:10.1016/j.polymer.2010.08.014.

683 [28] J.P. Kalish, K. Aou, X. Yang, S.L. Hsu. Spectroscopic and thermal analyses of α′ and α
684 crystalline forms of poly(L-lactic acid). Polymer. 52 (2011) 814-821.
685 doi:10.1016/j.polymer.2010.12.042.

686 [29] S.Z.D. Cheng, Z.Q. Wu, B. Wunderlich. Glass transition and melting behavior of
687 poly(thio-1,4-phenylene). Macromolecules. 20 (1987) 2802-2810. doi:10.1021/ma00177a028.

688 [30] E. Maemura, M. Cakmak, J.L. White. Characterization of Crystallinity and Orientation in
689 Poly-p-Phenylene Sulfide. International Polymer Processing. 3 (1988) 79-85.
690 doi:10.3139/217.880079.

691 [31] P. Huo, P. Cebe. Effects of thermal history on the rigid amorphous phase in
692 poly(phenylene sulfide). Colloid & Polymer Science. 270 (1992) 840-852.
693 doi:10.1007/BF00657728.

694 [32] G.Z. Papageorgiou, V. Tsanaktsis, D.N. Bikiaris. Synthesis of poly(ethylene
695 furandicarboxylate) polyester using monomers derived from renewable resources: thermal
696 behavior comparison with PET and PEN. Phys. Chem. Chem. Phys. 16 (2014) 7946-7958.
697 doi:10.1039/C4CP00518J.

698 [33] G. Stoclet, G. Gobius du Sart, B. Yeniad, S. de Vos, J.M. Lefebvre. Isothermal
699 crystallization and structural characterization of poly(ethylene-2,5-furanoate). Polymer. 72
700 (2015) 165-176. doi:10.1016/j.polymer.2015.07.014.

701 [34] J.G. van Berkel, N. Guigo, J.J. Kolstad, L. Sipos, B. Wang, M.A. Dam, N. Sbirrazzuoli.
702 Isothermal Crystallization Kinetics of Poly (Ethylene 2,5-Furandicarboxylate): Isothermal
703 Crystallization Kinetics of Poly (Ethylene 2,5-Furandicarboxylate). Macromolecular
704 Materials and Engineering. 300 (2015) 466-474. doi:10.1002/mame.201400376.

705 [35] G.Z. Papageorgiou, V. Tsanaktsis, D.G. Papageorgiou, S. Exarhopoulos, M.
706 Papageorgiou, D.N. Bikiaris. Evaluation of polyesters from renewable resources as
707 alternatives to the current fossil-based polymers. Phase transitions of poly(butylene 2,5-furan-
708 dicarboxylate). Polymer. 55 (2014) 3846-3858. doi:10.1016/j.polymer.2014.06.025.

709 [36] E.W. Fischer, H.J. Sterzel, G. Wegner. Investigation of the structure of solution grown
710 crystals of lactide copolymers by means of chemical reactions. Colloid and Polymer Science.
711 251 (11) (1973) 980-990. doi: 10.1007/BF01498927.

712 [36] T. Okada, L. Mandelkern. Effect of morphology and degree of crystallinity on the
713 infrared absorption spectra of linear polyethylene. Journal of Polymer Science Part A-2:
714 Polymer Physics. 5 (1967) 239-262. doi:10.1002/pol.1967.160050201.

715 [37] X. Hu, D. Kaplan, P. Cebe. Determining Beta-Sheet Crystallinity in Fibrous Proteins by
716 Thermal Analysis and Infrared Spectroscopy. Macromolecules. 39 (2006) 6161-6170.
717 doi:10.1021/ma0610109.

718 [38] C.E. Miller, B.E. Eichinger. Determination of Crystallinity and Morphology of Fibrous
719 and Bulk Poly(ethylene terephthalate) by Near-Infrared Diffuse Reflectance Spectroscopy.
720 Applied Spectroscopy. 44 (1990) 496-504. doi:10.1366/0003702904086173.

721 [39] S.-F. Yao, X.-T. Chen, H.-M. Ye. Investigation of Structure and Crystallization Behavior
722 of Poly(butylene succinate) by Fourier Transform Infrared Spectroscopy. The Journal of
723 Physical Chemistry B. 121 (2017) 9476-9485. doi:10.1021/acs.jpcb.7b07954.

724 [40] B.H. Stuart. Polymer crystallinity studied using Raman spectroscopy. Vibrational
725 Spectroscopy. 10 (1996) 79-87. doi:10.1016/0924-2031(95)00042-9.

726 [41] A. Nielsen, D. Batchelder, R. Pyrz. Estimation of crystallinity of isotactic polypropylene
727 using Raman spectroscopy. Polymer. 43 (2002) 2671-2676. doi:10.1016/S0032-
728 3861(02)00053-8.

729 [42] F. Rull, A.C. Prieto, J.M. Casado, F. Sobron, H.G.M. Edwards. Estimation of
730 crystallinity in polyethylene by Raman spectroscopy. Journal of Raman Spectroscopy. 24
731 (1993) 545-550. doi:10.1002/jrs.1250240813.

732 [43] L.S. Taylor, G. Zografi. The Quantitative Analysis of Crystallinity Using FT-Raman
733 Spectroscopy. Pharmaceutical Research. 15 (5) (1998) 755-761.
734 https://doi.org/10.1023/A:1011979221685.

735 [44] G.R. Strobl, W. Hagedorn. Raman spectroscopic method for determining the crystallinity
736 of polyethylene. Journal of Polymer Science: Polymer Physics Edition. 16 (1978) 1181-1193.
737 doi:10.1002/pol.1978.180160704.

738 [45] K. Schenzel, S. Fischer, E. Brendler. New Method for Determining the Degree of
739 Cellulose I Crystallinity by Means of FT Raman Spectroscopy. Cellulose. 12 (2005) 223-231.
740 doi:10.1007/s10570-004-3885-6.

741 [46] P. Cebe, X. Hu, D.L. Kaplan, E. Zhuravlev, A. Wurm, D. Arbeiter, C. Schick. Beating
742 the Heat - Fast Scanning Melts Silk Beta Sheet Crystals. Scientific Reports. 3 (2013) 1130.
743 doi: 10.1038/srep01130.

744 [47] Y. Corvis, A. Wurm, C. Schick, P. Espeau. Vitreous State Characterization of
745 Pharmaceutical Compounds Degrading upon Melting by Using Fast Scanning Calorimetry.
746 The Journal of Physical Chemistry B. 119 (2015) 6848-6851. doi:10.1021/acs.jpcb.5b03041.

747 [48] J.A.S. Puente, A. Esposito, F. Chivrac, E. Dargent. Effects of Size and Specific Surface
748 Area of Boron Nitride Particles on the Crystallization of Bacterial Poly(3-hydroxybutyrate- *co*
749 -3-hydroxyvalerate). Macromolecular Symposia. 328 (2013) 8-19.
750 doi:10.1002/masy.201350601.

751 [49] J.A.S. Puente, A. Esposito, F. Chivrac, E. Dargent. Effect of boron nitride as a nucleating
752 agent on the crystallization of bacterial poly(3-hydroxybutyrate). Journal of Applied Polymer
753 Science. 128 (2013) 2586-2594. doi:10.1002/app.38182.

754 [50] Y. Kong, J.N. Hay. The measurement of the crystallinity of polymers by DSC. Polymer.
755 43 (2002) 3873-3878. doi:10.1016/S0032-3861(02)00235-5.

756 [51] A. Toda, R. Androsch, C. Schick. Insights into polymer crystallization and melting from
757 fast scanning chip calorimetry. Polymer. 91 (2016) 239-263.
758 doi:10.1016/j.polymer.2016.03.038.

759 [52] A.A. Minakov, D.A. Mordvintsev, C. Schick. Melting and reorganization of
760 poly(ethylene terephthalate) on fast heating (1000 K/s). Polymer. 45 (2004) 3755-3763.
761 doi:10.1016/j.polymer.2004.03.072.

762 [53] S. Adamovsky, A. Minakov, C. Schick. Scanning microcalorimetry at high cooling rate.
763 Thermochimica Acta. 403 (2003) 55-63. doi:10.1016/S0040-6031(03)00182-5.

764 [54] F. De Santis, S. Adamovsky, G. Titomanlio, C. Schick. Scanning Nanocalorimetry at
765 High Cooling Rate of Isotactic Polypropylene. Macromolecules. 39 (2006) 2562-2567.
766 doi:10.1021/ma052525n.

767 [55] A. Esposito, N. Delpouve, V. Causin, A. Dhotel, L. Delbreilh, E. Dargent. From a Three-
768 Phase Model to a Continuous Description of Molecular Mobility in Semicrystalline
769 Poly(hydroxybutyrate-*co*-hydroxyvalerate). Macromolecules. 49 (2016) 4850-4861.
770 doi:10.1021/acs.macromol.6b00384.

771 [56] M. Pyda, A. Boller, J. Grebowicz, H. Chuah, B.V. Lebedev, B. Wunderlich. Heat
772 capacity of poly(trimethylene terephthalate). Journal of Polymer Science Part B: Polymer
773 Physics. 36 (1998) 2499-2511. doi:10.1002/(SICI)1099-0488(199810)36:14<2499::AID-
774 POLB4>3.0.CO;2-O.

775 [57] B. Wunderlich. Reversible crystallization and the rigid amorphous phase in
776 semicrystalline macromolecules. Progress in Polymer Science. 28 (2003) 383-450.
777 doi:10.1016/S0079-6700(02)00085-0.

778 [58] H. Chen, P. Cebe. Vitrification and Devitrification of Rigid Amorphous Fraction of PET
779 during Quasi-Isothermal Cooling and Heating. Macromolecules. 42 (2009) 288-292.
780 doi:10.1021/ma802104a.

781 [59] B. Wunderlich, A. Mehta. Macromolecular nucleation. Journal of Polymer Science:
782 Polymer Physics Edition. 12 (1974) 255-263. doi:10.1002/pol.1974.180120203.

783 [60] R. Androsch, B. Wunderlich. The link between rigid amorphous fraction and crystal
784 perfection in cold-crystallized poly(ethylene terephthalate). Polymer. 46 (2005) 12556-12566.
785 doi:10.1016/j.polymer.2005.10.099.

786 [61] M. Arnoult, E. Dargent, J.F. Mano. Mobile amorphous phase fragility in semi-crystalline
787 polymers: Comparison of PET and PLLA. Polymer. 48 (2007) 1012-1019.
788 doi:10.1016/j.polymer.2006.12.053.

789 [62] C. Schick, A. Wurm, A. Mohammed. Formation and disappearance of the rigid
790 amorphous fraction in semicrystalline polymers revealed from frequency dependent heat
791 capacity. Thermochimica Acta. 396 (2003) 119-132. doi:10.1016/S0040-6031(02)00526-9.

792 [63] M.C. Righetti, E. Tombari, M. Angiuli, M.L.D. Lorenzo. Enthalpy-based determination
793 of crystalline, mobile amorphous and rigid amorphous fractions in semicrystalline polymers.
794 Thermochimica Acta. 462 (2007) 15-24. doi:10.1016/j.tca.2007.06.003.

795 [64] A. Guinault, C. Sollogoub, V. Ducruet, S. Domenek. Impact of crystallinity of
796 poly(lactide) on helium and oxygen barrier properties. European Polymer Journal. 48 (2012)
797 779-788. doi:10.1016/j.eurpolymj.2012.01.014.

798 [65] T.L. Nguyen, F. Bédoui, P.-E. Mazeran, M. Guigon. Mechanical investigation of
799 confined amorphous phase in semicrystalline polymers: Case of PET and PLA. Polymer
800 Engineering & Science. 55 (2015) 397-405. doi:10.1002/pen.23896.

801 [66] S. Martín, M.T. Expósito, J.F. Vega, J. Martínez-Salazar. Microstructure and properties
802 of branched polyethylene: Application of a three-phase structural model. Journal of Applied
803 Polymer Science. 128 (2013) 1871-1878. doi:10.1002/app.38290.

804 [67] B.G. Olson, J. Lin, S. Nazarenko, A.M. Jamieson. Positron Annihilation Lifetime
805 Spectroscopy of Poly(ethylene terephthalate): Contributions from Rigid and Mobile
806 Amorphous Fractions. Macromolecules. 36 (2003) 7618-7623. doi:10.1021/ma034813u.

807 [68] M. Drieskens, R. Peeters, J. Mullens, D. Franco, P.J. Lemstra, D.G. Hristova-Bogaerds.
808 Structure versus properties relationship of poly(lactic acid). I. Effect of crystallinity on barrier
809 properties. Journal of Polymer Science Part B: Polymer Physics. 47 (2009) 2247-2258.
810 doi:10.1002/polb.21822.

811 [69] I. Kolesov, R. Androsch. The rigid amorphous fraction of cold-crystallized polyamide 6,
812 Polymer. 53 (2012) 4770-4777. doi:10.1016/j.polymer.2012.08.017.

813 [70] S. Fernandes Nassar, A. Guinault, N. Delpouve, V. Divry, V. Ducruet, C. Sollogoub, S.
814 Domenek. Multi-scale analysis of the impact of polylactide morphology on gas barrier
815 properties. Polymer. 108 (2017) 163-172. doi:10.1016/j.polymer.2016.11.047.

816 [71] C. Schick, A. Wurm, A. Mohamed. Vitrification and devitrification of the rigid
817 amorphous fraction of semicrystalline polymers revealed from frequency-dependent heat
818 capacity. Colloid and Polymer Science. 279 (2001) 800-806. doi:10.1007/s003960100507.

819 [72] M.C. Righetti, D. Prevosto, E. Tombari. Time and Temperature Evolution of the Rigid
820 Amorphous Fraction and Differently Constrained Amorphous Fractions in PLLA.
821 Macromolecular Chemistry and Physics. 217 (2016) 2013-2026.
822 doi:10.1002/macp.201600210.

823 [73] M.C. Righetti, E. Tombari. Crystalline, mobile amorphous and rigid amorphous fractions
824 in poly(L-lactic acid) by TMDSC. Thermochimica Acta. 522 (2011) 118-127.
825 doi:10.1016/j.tca.2010.12.024.

826 [74] S.F. Nassar, S. Domenek, A. Guinault, G. Stoclet, N. Delpouve, C. Sollogoub. Structural
827 and Dynamic Heterogeneity in the Amorphous Phase of Poly(L,L-lactide) Confined at the
828 Nanoscale by the Coextrusion Process. Macromolecules. 51 (2018) 128-136.
829 doi:10.1021/acs.macromol.7b02188.

830 [75] F. Hamonic, V. Miri, A. Saiter, E. Dargent. Rigid amorphous fraction versus oriented
831 amorphous fraction in uniaxially drawn polyesters. European Polymer Journal. 58 (2014) 233-
832 244. doi:10.1016/j.eurpolymj.2014.06.014.

833 [76] D.F. Miranda, C. Yin, S. Zhang, J. Runt. Fluoropolymer microstructure and dynamics:
834 Influence of molecular orientation induced by uniaxial drawing. Polymer. 91 (2016) 211-221.
835 doi:10.1016/j.polymer.2016.03.057.

836 [77] P. Huo, P. Cebe, Effects of thermal history on the rigid amorphous phase in poly
837 (phenylene sulfide), Colloid and Polymer Science. 270 (1992) 840–852.
838 doi:10.1007/BF0065772 8.

839 [78] A.A. Minakov, A. Wurm, C. Schick. Superheating in linear polymers studied by ultrafast
840 nanocalorimetry. Eur. Phys. J. E. 23 (2007) 43-53. doi: 10.1140/epje/i2007-10173-8.

841 [79] J. Menczel, B. Wunderlich. Heat capacity hysteresis of semicrystalline macromolecular
842 glasses. Journal of Polymer Science: Polymer Letters Edition. 19 (1981) 261-264.
843 doi:10.1002/pol.1981.130190506.

844 [80] Q. Ma, G. Georgiev, P. Cebe. Constraints in semicrystalline polymers: Using quasi-
845 isothermal analysis to investigate the mechanisms of formation and loss of the rigid
846 amorphous fraction. Polymer. 52 (2011) 4562-4570. doi:10.1016/j.polymer.2011.08.006.

847 [81] M. Kanchanasopa, E. Manias, J. Runt. Solid-State Microstructure of Poly(L-lactide) and
848 L-Lactide/meso-Lactide Random Copolymers by Atomic Force Microscopy (AFM).
849 Biomacromolecules. 4 (2003) 1203-1213. doi:10.1021/bm034063w.

850 [82] C. Santa Cruz, N. Stribeck, H. G. Zachmann, F. J. Baltá Calleja. Novel Aspects in the
851 Structure of Polyethylene terephthalate) As Revealed by Means of Small-Angle X-ray
852 Scattering. Macromolecules. 24 (1991) 5980-5990. doi: 10.1021/ma00022a013.

853 [83] A. Toda, M. Konishi, An evaluation of thermal lags of fast-scan microchip DSC with
854 polymer film samples, Thermochimica Acta. 589 (2014) 262–269.
855 doi:10.1016/j.tca.2014.05.038.

856 [84] C. Schick, V. Mathot (Eds.). Fast Scanning Calorimetry. Springer International
857 Publishing, Rostock, Germany, 2016. doi:10.1007/978-3-319-31329-0.

858 [85] J.E.K. Schawe, Measurement of the thermal glass transition of polystyrene in a cooling
859 rate range of more than six decades, Thermochimica Acta. 603 (2015) 128–134.
860 doi:10.1016/j.tca.2014.05.025.

861 [86] J.E.K. Schawe, Description of thermal relaxation of polystyrene close to the thermal
862 glass transition, Journal of Polymer Science Part B: Polymer Physics. 36 (1998) 2165–2175.
863 doi:10.1002/(SICI)1099-0488(19980915)36:12<2165::AID-POLB14>3.0.CO;2-Y.

864 [87] A. Dhotel, B. Rijal, L. Delbreilh, E. Dargent, A. Saiter, Combining Flash DSC, DSC and
865 broadband dielectric spectroscopy to determine fragility, Journal of Thermal Analysis and
866 Calorimetry. 121 (2015) 453–461. doi:10.1007/s10973-015-4650-9.

867 [88] X. Monnier, A. Saiter, E. Dargent, Vitrification of PLA by fast scanning calorimetry:
868 Towards unique glass above critical cooling rate?, Thermochimica Acta. 658 (2017) 47–54.
869 doi:10.1016/j.tca.2017.10.019.

870 [89] Lacey, A.A.; Price, D.M.; Reading, M.; Theory and Practice of Modulated Temperature
871 Differential Scanning Calorimetry. In Modulated Temperature Differential Scanning
872 Calorimetry; Springer: 2006; pp 1-81.

873 [90] V.B.F. Mathot. Temperature dependence of some thermodynamic functions for
874 amorphous and semi-crystalline polymers. Polymer. 25 (1984) 579–599. doi:10.1016/0032-
875 3861(84)90025-9.

876 [91] V.B.F. Mathot (Ed.). Thermal Characterization of States of Matter, in Calorimetry and
877 Thermal Analysis of Polymers (1994). Hanser/Gardner Publications, Cincinnati, OH USA.

878 [92] J. Zhang, Y. Duan, H. Sato, H. Tsuji, I. Noda, S. Yan, Y. Ozaki. Crystal Modifications
879 and Thermal Behavior of Poly(L-lactic acid) Revealed by Infrared Spectroscopy.
880 Macromolecules. 38 (2005) 8012-8021. doi:10.1021/ma051232r.

881 [93] L. Martino, N. Guigo, J.G. van Berkel, J.J. Kolstad, N. Sbirrazzuoli. Nucleation and Self-
882 Nucleation of Bio-Based Poly(ethylene 2,5-furandicarboxylate) Probed by Fast Scanning
883 Calorimetry. Macromolecular Materials and Engineering. 301 (2016) 586-596.
884 doi:10.1002/mame.201500418.

885 [94] J. Ma, X. Yu, J. Xu, Y. Pang. Synthesis and crystallinity of poly(butylene 2,5-
886 furandicarboxylate). Polymer. 53 (2012) 4145-4151. doi:10.1016/j.polymer.2012.07.022.

887 [95] M.L. Di Lorenzo. Calorimetric analysis of the multiple melting behavior of poly(L-lactic
888 acid). Journal of Applied Polymer Science. 100 (2006) 3145-3151. doi:10.1002/app.23136.

889 [96] P. Pan, W. Kai, B. Zhu, T. Dong, Y. Inoue. Polymorphous Crystallization and Multiple
890 Melting Behavior of Poly(L-lactide): Molecular Weight Dependence. Macromolecules. 40
891 (2007) 6898-6905. doi:10.1021/ma071258d.

892 [97] M. Yasuniwa, S. Tsubakihara, Y. Sugimoto, C. Nakafuku. Thermal analysis of the
893 double-melting behavior of poly(L-lactic acid). Journal of Polymer Science Part B: Polymer
894 Physics. 42 (2004) 25-32. doi:10.1002/polb.10674.

895 [98] A.P. Melnikov, M. Rosenthal, A.I. Rodygin, D. Doblas, D.V. Anokhin, M. Burghammer,
896 D.A. Ivanov. Re-exploring the double-melting behavior of semirigid-chain polymers with an
897 in-situ combination of synchrotron nano-focus X-ray scattering and nanocalorimetry.
898 European Polymer Journal. 81 (2016) 598-606. doi:10.1016/j.eurpolymj.2015.12.031.

[99] G.W.H. Höhne, Another approach to the Gibbs-Thomson equation and the melting point of polymers and oligomers, Polymer. 43 (2002) 4689-4698. doi:10.1016/S0032-3861(02)00305-1.

[100] A. Seidel, Characterization and Analysis of Polymers, John Wiley & Sons, 2008, p.755.

[101] N.S. Murthy, S.T. Correale, H. Minor, Structure of the amorphous phase in crystallizable polymers: poly(ethylene terephthalate), Macromolecules. 24 (1991) 1185–1189. doi:10.1021/ma00005a033.

[102] J.F. Mano, Structural evolution of the amorphous phase during crystallization of poly (l-lactic acid): A synchrotron wide-angle X-ray scattering study, Journal of Non-Crystalline Solids. 353 (2007) 2567–2572. doi:10.1016/j.jnoncrysol.2007.04.022.

[103] N.S. Murthy, H. Minor, General procedure for evaluating amorphous scattering and crystallinity from X-ray diffraction scans of semicrystalline polymers, Polymer. 31 (1990) 996–1002. doi:10.1016/0032-3861(90)90243-R.

[104] J.D. Hoffman. Regime III crystallization in melt-crystallized polymers: The variable cluster model of chain folding. Polymer. 24 (1983) 3-26. doi:10.1016/0032-3861(83)90074-5.

[105] I. Okazaki, B. Wunderlich. Modulated differential scanning calorimetry in the glass transition region, V. activation energies and relaxation times of poly(ethylene terephthalate)s. Journal of Polymer Science Part B: Polymer Physics. 34 (1996) 2941-2952. doi:10.1002/(SICI)1099-0488(199612)34:17<2941::AID-POLB7>3.0.CO;2-T.

[106] M. van Drongelen, T. Meijer-Vissers, D. Cavallo, G. Portale, G.V. Poel, R. Androsch. Microfocus wide-angle X-ray scattering of polymers crystallized in a fast scanning chip calorimeter. Thermochimica Acta. 563 (2013) 33-37. doi:10.1016/j.tca.2013.04.007.

[107] D. Baeten, V.B.F. Mathot, T.F.J. Pijpers, O. Verkinderen, G. Portale, P. Van Puyvelde, B. Goderis. Simultaneous Synchrotron WAXD and Fast Scanning (Chip) Calorimetry: On the (Isothermal) Crystallization of HDPE and PA11 at High Supercoolings and Cooling Rates up to 200 °C s^{-1}. Macromolecular Rapid Communications. 36 (2015) 1184-1191. doi:10.1002/marc.201500081.

GRAPHICAL ABSTRACT

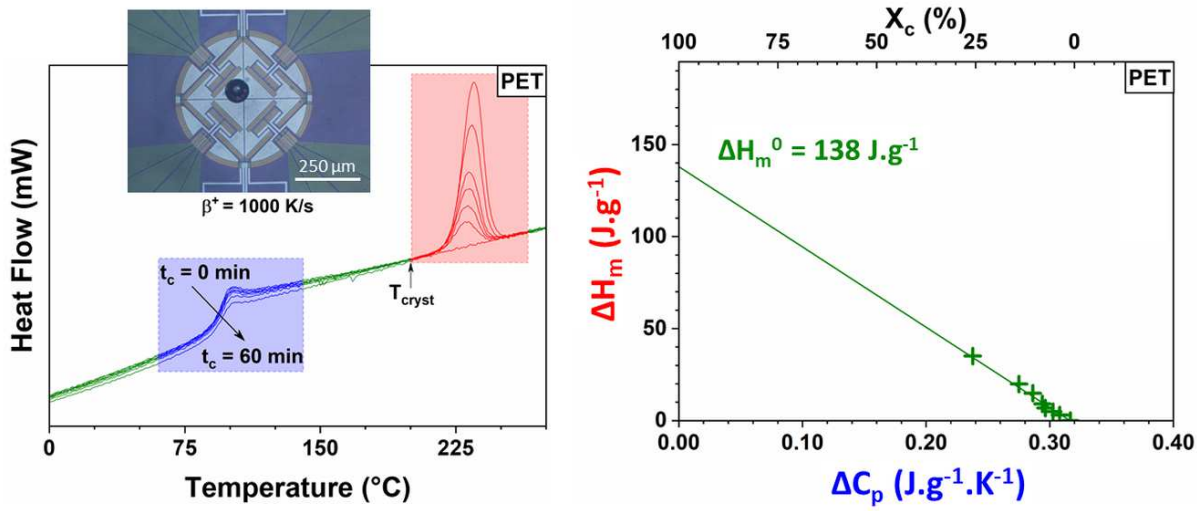

HIGHLIGHTS

- A new procedure to calculate the equilibrium enthalpy of melting is proposed.
- Fast Scanning Calorimetry was used to obtain the equilibrium enthalpy of melting.
- Nanoscale samples were crystallized *in situ* on FSC sensors.
- Annealing conditions reduced the coupling between amorphous and crystalline phases.
- Agreements and divergences with cross-comparison methods are discussed.